

First-principles calculations on elastic, magnetoelastic, and phonon properties of Ni_2FeGa magnetic shape memory alloys

Wangqiang He(贺王强), Houbing Huang(黄厚兵), Zhuhong Liu(柳祝红), Xingqiao Ma(马星桥)
Citation: Chin. Phys. B . 2018, 27(1): 016201. **doi:** 10.1088/1674-1056/27/1/016201

Journal homepage: http://cpb.iphy.ac.cn; http://iopscience.iop.org/cpb

What follows is a list of articles you may be interested in

Effects of alloying element on stabilities, electronic structures, and mechanical properties of Pd-based superalloys

Pei Yan(闫佩), Xiao-Yu Chong(种晓宇), Ye-Hua Jiang(蒋业华), Jing Feng(冯晶)
Chin. Phys. B . 2017, 26(12): 126202. **doi:** 10.1088/1674-1056/26/12/126202

First-principles study of the new potential photovoltaic absorber: Cu_2MgSnS_4 compound

Belmorsli Bekki, Kadda Amara, Mohammed El Keurti
Chin. Phys. B . 2017, 26(7): 076201. **doi:** 10.1088/1674-1056/26/7/076201

Stability, elastic anisotropy, and electronic properties of Ca_2C_3

Quan Zhang(张权), Qun Wei(魏群), Hai-Yan Yan(闫海燕), Xuan-Min Zhu(朱轩民), Jun-Qin Zhang(张军琴), Xiao-Fei Jia(贾晓菲), Rong-Hui Yao(姚荣辉)
Chin. Phys. B . 2017, 26(6): 066201. **doi:** 10.1088/1674-1056/26/6/066201

Elastic and thermodynamic properties of vanadium nitride under pressure and the effect of metallic bonding on its hardness

Pu Chun-Ying, Zhou Da-Wei, Bao Dai-Xiao, Lu Cheng, Jin Xi-Lian, Su Tai-Chao, Zhang Fei-Wu
Chin. Phys. B . 2014, 23(2): 026201. **doi:** 10.1088/1674-1056/23/2/026201

Influence of strain and electric field on the properties of silicane

Cheng Gang, Liu Peng-Fei, Li Zi-Tao
Chin. Phys. B . 2013, 22(4): 046201. **doi:** 10.1088/1674-1056/22/4/046201

First-principles calculations on elastic, magnetoelastic, and phonon properties of Ni_2FeGa magnetic shape memory alloys*

Wangqiang He(贺王强)†, Houbing Huang(黄厚兵)‡, Zhuhong Liu(柳祝红), and Xingqiao Ma(马星桥)

Department of Physics, University of Science and Technology Beijing, Beijing 100083, *China*

(Received 9 July 2017; revised manuscript received 26 August 2017; published online 28 November 2017)

The elastic, magnetoelastic, and phonon properties of Ni_2FeGa were investigated through first-principles calculations. The obtained elastic and phonon dispersion curves for the austenite and martensite phases agree well with available theoretical and experimental results. The isotropic elastic moduli are also predicted along with the polycrystalline aggregate properties including the bulk modulus, shear modulus, Young's modulus, and Poisson's ratio. The Pugh ratio indicates that Ni_2FeGa shows ductility, especially the austenite phase, which is consistent with the experimental results. The Debye temperatures of the Ni_2FeGa in the austenite and martensite phases are 344 K and 392 K, respectively. It is predicted that the magnetoelastic coefficient is -5.3×10^6 J/m^3 and magnetostriction coefficient is between 135 and 55 ppm in the Ni_2FeGa austenite phase.

Keywords: Ni_2FeGa, elastic constants, first-principles calculations, magnetoelastic coefficients

PACS: 62.20.de, 62.20.dj, 63.10.+a, 75.47.Np **DOI:** 10.1088/1674-1056/27/1/016201

1. Introduction

Ferromagnetic shape memory alloys (FSMAs) such as Ni_2MnGa have received continuous attention from a technological perspective as smart materials for application in sensors and actuators.[1,2] Ni_2MnGa shows magnetic-field-induced strains (MFISs) up to 12% by the rearrangement of twin variants in the non-modulated (NM) martensitic phase.[3] However, the application of Ni_2MnGa alloys is restricted by their brittleness and low transition temperatures. Recently, Ni_2FeGa alloys have emerged as an alternative to Ni_2MnGa alloys owing to their better ductility.[4] This alloy exhibits a Curie temperature of 430 K and a martensitic transformation temperature of 142 K. Different martensitic phases such as the modulated 5M, 6M, and 7M phases would be formed during the phase transition upon cooling.[5,6] The MFISs of the Ni_2FeGa alloys are approximately 0.02%–0.3% in modulated martensite,[7,8] and an MFIS of about 2% has been achieved in the non-layered $L1_0$ martensite of the Ni–Fe–Ga–Co alloys since the extra Co atoms improve the magnetic anisotropy constant, Curie temperature, and transformation temperature of the compounds.[4] The microstructural features and structural phase transition in the Ni_2FeGa and Ni–Fe–Ga–Co alloys have been systematically investigated by means of transmission electron microscopy.[9,10] Recently, Liu *et al.*[11,12] reported that the Ni–Fe–Ga alloys have become one of the potential candidates for solid-state mechanical cooling applications because they show large reversible elastocaloric effects.

Theoretical investigations based on density functional theory prove to be a powerful tool; for instance, to predict the structural, elastic, electronic, and thermodynamic properties of materials such as NB_2,[13] cubic-NbH_2 hydride,[14] sulfur-doped GaSe,[15] and $CdSe_{1-x}Te_x$.[16] Several *ab initio* investigations have been carried out on the structural, electronic, elastic, and magnetic properties of stoichiometric[17–19] and off-stoichiometric[20,21] Ni_2FeGa alloys in the austenite and martensite phases. Moreover, several theoretical studies aiming to understand the origin of the martensitic phase transformation have closely correlated the phonon anomaly in the austenite phase with Fermi surface nesting and electron–phonon coupling.[22,23] However, only a few theoretical studies have been conducted to date on the isotropic elastic moduli, Debye temperatures, and magnetoelastic properties of the Ni_2FeGa alloys. Studying the isotropic elastic moduli is very important because the mechanical and thermodynamic properties can be obtained by calculating the elastic constants.[24] Furthermore, phase-field simulations have been used to simulate the formation and evolution of magnetoelastic domains under combined mechanical and magnetic loading,[25] the stress–strain behaviors, and the magnetic-field-induced strain behaviors[26] of the Ni_2MnGa alloys. The magnetoelastic coefficient is an important parameter for establishing the thermodynamic potential in phase-field simulations, and it is usually obtained by fitting the experimental measurements.[26,27] Therefore, it is meaningful for multi-scale simulations that the first-principles calculations provide the parameters such as the magnetoelastic coefficients for the phase-field simulations to build a model of the thermodynamic potential.[28] The pur-

*Project supported by the National Natural Science Foundation of China (Grant Nos. 11174030 and 11504020) and the Fundamental Research Funds for the Central Universities of China (Grant No. FRF-TP-16-064A1, 06500031).

†Corresponding author. E-mail: hewangqiang@yeah.net

‡Corresponding author. E-mail: hbhuang@ustb.edu.cn

© 2018 Chinese Physical Society and IOP Publishing Ltd

pose of the present work is to provide a first-principles-based description of the magnetoelastic coupling in ferromagnetic shape memory alloys, which can be used as a basis for further studies of this important class of materials. In this work, we present the investigations of the isotropic elastic moduli and the magnetoelastic properties of stoichiometric Ni_2FeGa alloys through *ab initio* calculations. We approach this investigation by modeling the austenite as a 16-atom $L2_1$ supercell. The phonon dispersions of the austenite and martensite structures were also calculated.

2. Computational details

The calculations were performed using the Vienna *ab initio* simulation package[29,30] (VASP) based on density functional theory. The electronic exchange and correlation were described within a spin-polarized generalized-gradient approximation (GGA), using the function proposed by Perdew, Burke, and Ernzerhof (PBE).[31,32] The Brillouin zone (BZ) was sampled with a special $11\times11\times11$ k-point mesh arranged in a Monkhorst–Pack scheme,[33] and the energy cutoff was set at 470 eV. The electron–ion interaction was as described in the projector augmented-wave (PAW) formalism, and Ni ($3d^84s^2$), Fe ($3d^74s^1$), and Ga ($3d^{10}4s^24p^1$) were treated as the valance states. For the calculation of the magnetocrystalline anisotropy energy, the spin–orbit coupling effect was considered, and the symmetry was switched off. The full self-consistent calculation of the spin–orbital interaction have been previously performed in the non-collinear model implemented by Hobbs *et al.*[34] and Marsman and Hafner[35] in the VASP.

The phonon calculations were performed using the finite displacement approaches with the phonopy[36,37] code. The Hellmann–Feynman forces were calculated using the VASP code and by applying Methfessel–Paxton smearing with a smearing parameter of $\sigma = 0.1$ eV to a $4\times4\times4$ k-point grid. The $2\times2\times2$ supercell for the austenite phase was generated by repeating the conventional unit cell (Fig. 1(a)) twice in each direction, and the $3\times3\times2$ supercell for the non-modulated (NM) martensite phase was generated with the conventional tetragonal cell shown in Fig. 1(b).

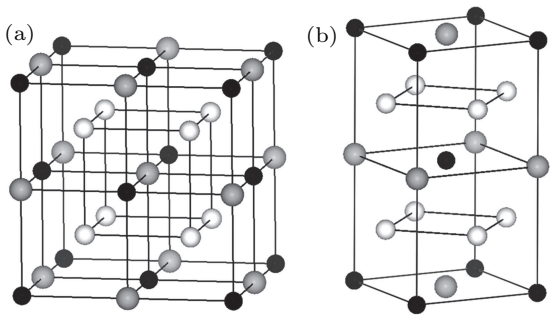


Fig. 1. (a) The $L2_1$ Heusler structure of Ni_2FeGa fabricated with the conventional unit cell, and (b) the conventional tetragonal cell used in the phonon calculations. The black, gray, and white circles in the pictures represent the Ni, Fe, and Ga atoms, respectively.

3. Results and discussion

3.1. Structural properties

Figure 1(a) shows the conventional cell representing the austenite phase of the Ni_2FeGa alloys. The stoichiometric Ni_2FeGa compound adopts an $L2_1$ structure, where Ni atoms occupy the sites (0.25, 0.25, 0.25) and (0.75, 0.75, 0.75), Ga atoms occupy the sites (0, 0, 0), and Fe atoms are located at (0.5, 0.5, 0.5), with 16 atoms per unit cell. To obtain the equilibrium structure of the austenite phase, we calculated the total energy of the unit cell for different volumes of the alloy and fitted it to the 4th-order Birch–Murnaghan equation of state (EoS). The calculated E–V relationship for the austenite phase is shown in Fig. 2. Table 1 lists the fitted parameters of the EoS, including the equilibrium lattice parameter, a, the bulk modulus, B, and the pressure derivative, B'. The predicted lattice constant of the austenite phase is 5.77 Å and is consistent with the experimental value of 5.76 Å[38] and other theoretical values 5.76 Å[17] and 5.77 Å.[23] The predicted bulk modulus, B, is 166.2 GPa, which also is in good agreement with other theoretical values of 165.1 GPa[17] and 164.7 GPa.[23] The total magnetic moment of the austenitic phase is 3.3 μ_B/f.u., which is in good agreement with previously obtained theoretical value of 3.29 μ_B/f.u..[17] The stability of the austenite phase with respect to the tetragonal distortions is explored and presented in Fig. 3. The total energy of the austenite Ni_2FeGa calculated with respect to the different tetragonal deformations shows two minima: one at $c/a = 0.9$, corresponding to

Table 1. Structural properties such as the lattice constant (a, in Å), total magnetic moment (μ, in μ_B/f.u.), bulk modulus (B, in GPa), and the pressure derivative (B') for the Ni_2FeGa austenite phase.

	a	μ	B	B'
This work	5.766	3.30	166.2	4.6
VASP[a]	5.76[a]	3.29[a]	165.1[a]	4.82[a]
QE[b]	5.77[b]		164.7[b]	5.32[b]
Expt.[c]	5.76[c]	3.03[c]		

[a]Ref. [17] by VASP calculations.
[b]Ref. [23] by QUANTUM ESPRESSO calculations.
[c]Ref. [38].

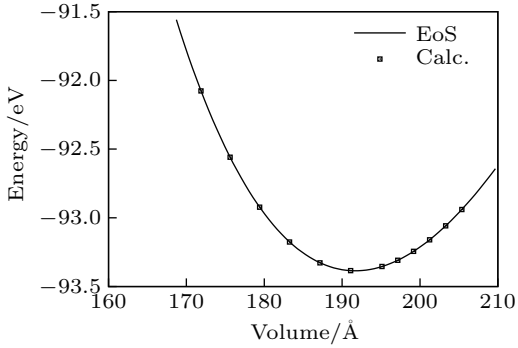


Fig. 2. The relationship between the calculated energy and volume. The solid curve represents the data from the E–V curves fitted according to the 4th-order Birch–Murnaghan equation of state (EoS). The dots represent the actual calculated results.

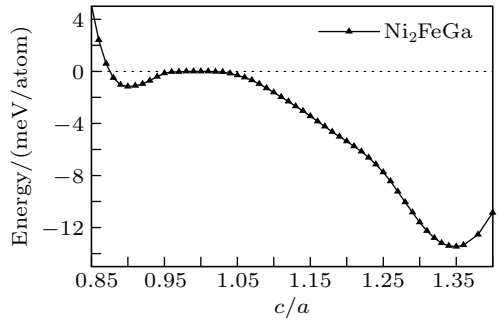


Fig. 3. The total energy of the austenite Ni_2FeGa calculated with respect to different tetragonal deformations, c/a.

the modulated martensite structure, the other at $c/a = 1.35$, corresponding to the NM martensite phase. The structures represented by both minima have lower energies than the cubic structure, which means that the cubic phase is unstable and that the tetragonal distortion enhances the phase stability. The differences between the energies of the cubic and NM tetragonal structures at $c/a = 0.9$ and 1.35 are about 1.2 and 13.5 meV/atom, respectively. Our calculated energy differences are in agreement with the previously reported results of 10.5[20] and 11 meV/atom, respectively.[17]

3.2. Elastic properties

First, the three independent elastic constants for the cubic phase and the six for the NM martensitic phase were calculated by the strain–stress method.[39] The stress calculations were conducted with 2 and 4 independent sets of strains for the cubic and NM tetragonal phases, respectively. The calculated results are listed in Table 2, and other theoretical values[17,20] as well as experimental values[38] are listed for comparison. It is noted that in the austenite phase, C_{11} is smaller than C_{12}, and the shear elastic constant, C' ($C' = \frac{C_{11}-C_{12}}{2}$) is negative, which is an important quantity that indicates the instability of the austenite phase.[40] Table 2 also shows that the elastic constants of the tetragonal martensite, Ni_2FeGa, satisfy the criteria for mechanical stabilities, indicating that the phase is mechanically stable. The mechanical stabilities for the cubic and tetragonal crystals are as follows.

Table 2. Calculated elastic constants and isotropic moduli (in GPa), Poisson's ratio (v), and Pugh ratio of Ni_2FeGa alloys. The available experimental data and other calculation results are also listed.

Phase		C_{11}	C_{33}	C_{12}	C_{13}	C_{44}	C_{66}	C'	B	G	E	v	B/G
Austenite	This work	163.8		168.1		106.5		–2.2	166.7	28.7	81.6	0.42	5.80
	VASP[a]	166.0		168.9		109.8		–1.5	168				
	VASP[b]	140.87		141.57		98.39		–0.35	141.34	58.89	155.13	0.32	2.39
	QE[c]	223				75		32					
	Expt.[d]	163		136.9		86		13	145.6				
Martensite NM	This work	247.6	211.1	90.7	142.6	92.2	40.4	78.5	161.8	61.0	162.6	0.33	2.65
	VASP[a]	248.5	207.1	96.0	158.1	104.8	45.3	76.3	169.8				

[a]Ref. [17].
[b]Ref. [20].
[c]Ref. [23] by QUANTUM ESPRESSO calculations.
[d]Ref. [38].

$$\begin{aligned} &C_{11}-C_{12}>0,\ \ C_{11}>0,\ \ C_{33}>0,\ \ C_{11}+2C_{12}>0,\\ &C_{11}-C_{12}>0,\ \ C_{11}+C_{33}-2C_{13}>0,\ \ C_{66}>0,\\ &(2C_{11}+C_{33}+2C_{12}+4C_{14})>0. \end{aligned} \tag{1}$$

The isotropic moduli such as the bulk modulus, B, shear modulus, G, Young's modulus, E, and the Poisson and Pugh ratios were obtained using the Voigt[41]–Reuss[42]–Hill[43] relations for polycrystalline materials. In calculating the moduli G and B, Voigt[41] assumed that homogeneous strain was maintained throughout the stressed samples. Reuss,[42] on the other hand, believed that homogeneous stress was maintained in all directions throughout the stressed samples. However, Hill[43] later proposed that the true values of the moduli should be given by the average of the Voigt and Reuss values. For simplicity, we only considered the tetragonal crystal structure. The bulk modulus calculated by the Voigt approximation is given by

$$B_{\mathrm{V}} = \frac{1}{9}(c_{11}+c_{22}+c_{33}) + \frac{2}{9}(c_{12}+c_{23}+c_{13}). \tag{2}$$

The shear modulus calculated by the Voigt approximation is given by

$$\begin{aligned} G_{\mathrm{V}} &= \frac{1}{15}(c_{11}+c_{22}+c_{33}) - \frac{1}{15}(c_{12}+c_{23}+c_{13})\\ &\quad + \frac{1}{5}(c_{44}+c_{55}+c_{66}). \end{aligned} \tag{3}$$

The bulk modulus calculated by the Reuss approximation is given by

$$\frac{1}{B_{\mathrm{R}}} = (s_{11}+s_{22}+s_{33}) + 2(s_{12}+s_{23}+s_{13}), \tag{4}$$

where s_{ij} are the elastic compliance constants.

The shear modulus calculated by the Reuss approximation is given by

$$\begin{aligned} \frac{15}{G_{\mathrm{R}}} &= 4(s_{11}+s_{22}+s_{33}) - 4(s_{12}+s_{23}-s_{13})\\ &\quad + 3(s_{44}+s_{55}+s_{66}), \end{aligned} \tag{5}$$

where

$$s_{11} = s_{22} = \frac{(c_{11}c_{33}-c_{13}^2)}{(c_{11}-c_{12})(c_{11}+c_{12})c_{33}-2c_{13}^2},$$

$$
\begin{aligned}
s_{33} &= \frac{(c_{11}+c_{12})}{(c_{11}+c_{12})c_{13}-2c_{13}^2},\\
s_{12} &= \frac{(c_{13}^2-c_{12}c_{33})}{(c_{11}-c_{12})(c_{11}+c_{12})c_{33}-2c_{13}^2},\\
s_{13} &= \frac{c_{13}}{2c_{13}^2-(c_{11}+c_{12})c_{33}},\\
s_{44} &= s_{55} = \frac{1}{c_{44}},\\
s_{66} &= \frac{1}{c_{66}}.
\end{aligned} \tag{6}
$$

B and G are typically calculated as the average of the shear moduli given by

$$
B = \frac{1}{2}(B_{\mathrm{R}}+B_{\mathrm{V}}), \quad G = \frac{1}{2}(G_{\mathrm{R}}+G_{\mathrm{V}}). \tag{7}
$$

The Young's modulus, E, and Poisson's ratio, ν, for an isotropic material are given by

$$
E = \frac{9BG}{2B+G}, \quad \upsilon = \frac{3B-2G}{2(3B+G)}. \tag{8}
$$

The important moduli for applications, i.e., the bulk and shear moduli, are calculated and are listed in Table 2. The bulk modulus, B, represents the resistance of the material to fracture, and the isotropic shear modulus, G, is related to the resistance of the material to plastic deformation. It should be noted that the bulk modulus ($B = 166.7$ GPa) calculated from the elastic constant (EC) of the austenite phase agrees well with those directly obtained by fitting with the Birch–Murnaghan EoS ($B = 166.2$ GPa), as listed in Table 1, which further demonstrates the accuracy of our elastic constant calculations.

According to the Pugh criteria,[44] a B/G ratio of 1.75 separates ductile and brittle materials; that is, ductile fcc metals all have a high B/G, whereas brittle bcc metals all have a low B/G.[45] All the phases we calculated were ductile since their Pugh ratio, $B/G > 1.75$. In Table 2, the Pugh ratio for Ni_2FeGa, 5.8, is larger than that for Ni_2MnGa, 3.93, revealing the more ductile nature of Ni_2FeGa. The smaller Poisson's ratio for the NM martensite phase, as listed in Table 2, indicated that the NM martensite phase was relatively stable against shear deformation.

The Debye temperature is an important fundamental parameter correlated to the physical properties of materials, such as the specific heat capacity and melting point. We calculated the Debye temperatures of Ni_2FeGa in the austenite and martensite phases from the average sound velocity, v_{m}, using the following relation and assuming a constant sound velocity. The Debye temperature is given by[46,47]

$$
\theta_D = 67.48\frac{r_0 B_0}{M}v_{\mathrm{m}}, \tag{9}
$$

and the average sound velocity, v_{m}, is approximated by the following equations:

$$
v_{\mathrm{m}} = \left[\frac{1}{3}\left(\frac{2}{v_{\mathrm{t}}^3}+\frac{1}{v_{\mathrm{l}}^3}\right)\right]^{-1/3},
$$

$$
v_{\mathrm{l}} = \left(\frac{3B+4G}{3\rho}\right)^{1/2}, \quad v_{\mathrm{t}} = \left(\frac{G}{\rho}\right)^{1/2}, \tag{10}
$$

where v_{l}, v_{t}, and v_{m} are the longitudinal, transverse, and average sound velocities of the isotropic material, respectively, and are listed in Table 3. Here, B and G are the polycrystalline bulk and shear moduli, respectively. The Debye temperatures of the austenite and martensite phases were 344 and 392 K, respectively, as listed in Table 3. It is noted that the Debye temperature for the austenitic phase is lower than that for the martensitic phase, which indicates that the specific heat, C_{p}, for austenite is higher than that for martensite.[24]

Table 3. The longitudinal sound velocity (v_{l}, in km/s), transverse sound velocity (v_{t}, in km/s), and average sound velocity (v_{m}, in km/s) calculated from the polycrystalline elastic modulus, and the Debye temperature (Θ_D, in K) obtained from the average sound velocity for the austenitic and NM martensitic Ni_2FeGa alloys.

Phase	v_{l}	v_{t}	v_{m}	Θ_D
Austenite	4.5	1.7	1.9	344
Martensite NM	4.9	2.5	2.7	392

3.3. Magnetoelastic properties

For small distortions in the cubic crystal lattice, the magnetoelastic energy, $K(\varepsilon)$,[48] is related to the uniaxial magnetocrystalline anisotropy energy (MAE) of the cubic structure. In the present work, the MAE is defined as $K = E_{110} - E_{001}$, where E_{110} and E_{001} are the total energies when the magnetization is in the [110] and [001] directions of the cubic phase, respectively.

$$
K(\varepsilon) = -\frac{3}{2}B_1\varepsilon + K_0. \tag{11}
$$

The total energy can be written as the sum of the elastic and magnetoelastic energies, E_{el} and E_{me}, respectively, which are assumed to be quadratic,[49]

$$
E_{\mathrm{tot}} = -\alpha B_1\varepsilon + C\varepsilon^2, \tag{12}
$$

where α is a constant that equals 1 for magnetization parallel to the tetragonal axis and 1/2 for magnetization perpendicular to the tetragonal axis, ε is the tetragonal distortion ($\varepsilon = 2/3(c/a-1)$), B_1 is the magnetoelastic coupling coefficient, and C is related to the elastic constant ($C = 3V_0C'/2$), where V_0 is the volume of the unit cell. The magnetostriction coefficient is defined as the strain that minimizes the total energy given by Eq. (12) and is given by the following formula:[50]

$$
\lambda_{100} = -\frac{B_1}{2C}. \tag{13}
$$

The magnetoelastic coupling coefficients, B_1, of the Ni_2MnGa and Ni_2FeGa alloys are determined from the slopes of the lines in the MAE versus ε plot in Fig. 4. The B_1 of Ni_2MnGa is 4.4×10^6 J/m^3, which was in agreement with

the B_1 of 4×10^6 J/m^3 obtained by fitting the experimental measurements in the previous phase-field simulation.[26] From the magnetoelastic coupling coefficient ($B_1 = -5.3 \times 10^6$ J/m^3) and shear elastic constant ($C' = 13$–32 GPa[23,38]) of the Ni_2FeGa, the magnetostriction coefficient of austenite Ni_2FeGa was calculated between 135 and 55 ppm by Eq. (13) and is listed in Table 4. To our knowledge, the neither the magnetoelastic coupling coefficient nor the magnetostriction coefficient of the Ni_2FeGa alloys has been previously reported. It is notable that the B_1 of Ni_2MnGa is positive while that of Ni_2FeGa is negative. In Fig. 4, the MAE of Ni_2MnGa changes from positive to negative when the tetragonal strain crosses $c/a = 1$, thus leading to a positive B_1, and the MAE of Ni_2FeGa changes from negative to positive, resulting in a negative B_1.

Table 4. Calculated magnetoelastic coefficient (B_1, in 10^6 J/m^3) and magnetostriction coefficient (λ_{100}) of Ni_2MnGa and Ni_2FeGa alloys.

Alloys		B_1	C'	$\lambda_{100}/10^{-6}$
Ni_2MnGa	This calculation	4.4	4.5–22	−(326–67)
	Theoretical values[a]		4.5–22	−(500–100)
	Phase field simulations[b]	4		
Ni_2FeGa	This calculation	−5.3	13–32	135–55

[a]Ref. [49]

[b]Ref. [26]

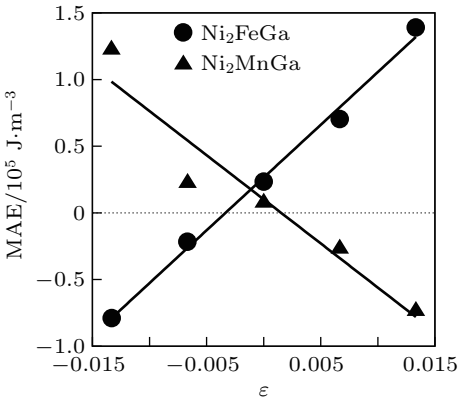


Fig. 4. The magnetocrystalline anisotropy energy (MAE) calculated as a function of the strain of the Ni_2MnGa and Ni_2FeGa alloys.

3.4. Phonon band structure calculations

The phonon dispersion curves and the total vibrational densities of states (VDOSs) calculated using GGA for the cubic and NM phases of Ni_2FeGa are shown in Figs. 5(a) and 5(b), respectively. The phonon dispersion curves in Fig. 5(a) predicted by our calculations are in agreement with those recently obtained in neutron diffraction experiments.[38] The transverse acoustical (TA) and optical branches in the [1 0 0] (G–X) direction were doubly degenerate owing to the symmetry of the cubic crystal, while the dispersion along the [1 1 0] (G–K) direction is composed of 3 acoustical and 9 optical non-degenerate branches. The negative phonon frequencies of the transverse acoustic mode (TA_2) branch completely softened along the [110] direction between the wave vectors $\zeta = 0$ and $\zeta = 0.75$ in Fig. 5(a), and this anomaly is usually related to Fermi surface nesting and electron–phonon coupling.[22] The appearance of the TA_2 acoustic phonon anomaly means that the cubic $L2_1$ structure is unstable at zero temperature, and the anomaly corresponds to the formation of modulated structures such as the 5M or 7M structures in the premartensite phase.[51] Pérez-Landazábal *et al.*[38] reported that the TA_2 branch along [110] direction of the nonstoichiometric $L2_1$ phase of Ni_2FeGa showed a slight softening due to inelastic neutron scattering around $\zeta = 0.35$. Satyananda *et al.*[22] reported softening at the wave vectors $\zeta = 0.58$ rather than between the wave vectors $\zeta = 0$ and $\zeta = 0.75$ obtained in our calculations because the linear response method of density functional perturbation theory (DFPT) was used in their calculations. Since the softening of the acoustic (TA_2) mode is related to a negative shear constant (C'), the appearance of the phenomenon indicates the structural instability of the Ni_2FeGa single crystal against shear deformation. Figure 5(b) reveals that all the phonon modes had real values in the whole Brillouin zone, indicating that the NM martensite phase in the Ni_2FeGa was dynamically stable. Therefore, the NM martensite phase was more stable than the austenite phase from the perspective of lattice dynamics.

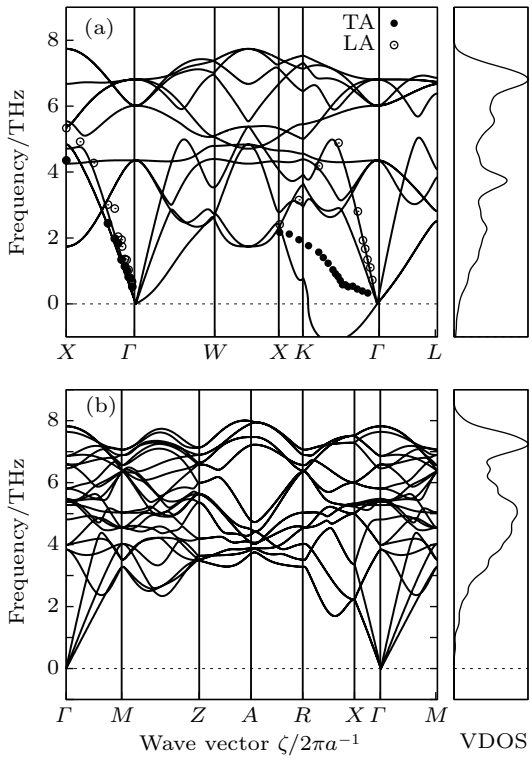


Fig. 5. Phonon band structure and vibrational density of states (VDOS) along high-symmetry lines in the first Brillouin zone for (a) cubic (b) non-modulated martensite Ni_2FeGa alloys. The circles indicate the neutron-scattering measurement data from Ref. [38]. The imaginary values of the phonon frequencies are plotted along the negative frequency axis.

4. Conclusions

In this work, the elastic, magnetoelastic, and phonon properties of the Ni_2FeGa system were investigated and compared to the available theoretical and experimental data. By fitting the total energy as a function of the volume with the Birch–Murnaghan EoS, the bulk modulus and the equilibrium lattice parameter are obtained. The bulk modulus (B), shear modulus (G), Young's modulus (E), and Poisson's ratio (ν) of the Ni_2FeGa are determined using the Voigt–Reuss–Hill approach, and the results were in good agreement with previous calculations. The Debye temperatures of the Ni_2FeGa in the austenite and martensite phases were 344 and 392 K, respectively. The magnetoelastic coefficient is -5.3×10^6 J/m^3, and the magnetostriction coefficient of the Ni_2FeGa austenite phase is between 135 and 55 ppm, as obtained by calculating the magnetocrystalline anisotropy energy—which can provide a helpful reference for further phase-field simulation work. The phonon dispersion curves and vibrational densities of states of the austenite and martensite phases were presented.

References

[1] Ullakko K, Huang J K, Kantner C, O'Handley R C and Kokorin V V 1996 *Appl. Phys. Lett.* **69** 1966
[2] Sozinov A, Likhachev A A, Lanska N and Ullakko K 2002 *Appl. Phys. Lett.* **80** 1746
[3] Sozinov A, Lanska N, Soroka A and Zou W 2013 *Appl. Phys. Lett.* **102** 021902
[4] Masdeu F, Pons J, Cesari E, Kustov S and Chumlyakov Y I 2008 *Appl. Phys. Lett.* **93** 152503
[5] Sutou Y, Kamiya N, Omori T, Kainuma R, Ishida K and Oikawa K 2004 *Appl. Phys. Lett.* **84** 1275
[6] Oikawa K, Ota T, Ohmori T, Tanaka Y, Morito H, Fujita A, Kainuma R, Fukamichi K and Ishida K 2002 *Appl. Phys. Lett.* **81** 5201
[7] Morito H, Fujita A, Fukamichi K, Kainuma R, Ishida K and Oikawa K 2003 *Appl. Phys. Lett.* **83** 4993
[8] Liu Z H, Zhang M, Cui Y T, Zhou Y Q, Wang W H, Wu G H, Zhang X X and Xiao G 2003 *Appl. Phys. Lett.* **82** 424
[9] Liu L, Fu S, Liu Z, Wu G, Sun X and Li J 2006 *J. Alloy Compd.* **425** 176
[10] Liu Q H, Liu J, Huang Y J, Hu Q D and Li J G 2013 *J. Alloy Compd.* **572** 186
[11] Xu Y, Lu B, Sun W, Yan A and Liu J 2015 *Appl. Phys. Lett.* **106** 201903
[12] Xiao F, Jin M, Liu J and Jin X 2015 *Acta Mater.* **96** 292
[13] Wu J H and Liu C X 2016 *Chin. Phys. Lett.* **33** 036202
[14] Liu X K 2013 *Chin. Phys. Lett.* **30** 066201
[15] Huang C B, Wu H X, Ni Y B, Wang Z Y, Qi M and Zhang C L 2016 *Chin. Phys. B* **25** 086201
[16] Shakil M Z, Shabbir Ahmed, Muhammad Raza-ur-rehman Hashmi, Choudhary M A and Iqbal T 2016 *Chin. Phys. B* **25** 076104
[17] Soykan C, Özdemir Kart S, Sevik C and Çağın T 2014 *J. Alloy Compd.* **611** 225
[18] Sahariah M B, Ghosh S, Singh C S, Gowtham S and Pandey R 2013 *J. Phys. Conden. Matt.* **25** 025502
[19] Liu Z H, Hu H N, Liu G D, Cui Y T, Zhang M, Chen J L, Wu G H and Xiao G 2004 *Phys. Rev. B* **69** 134415
[20] Chabungbam S, Borgohain P, Ghosh S, Singh N and Sahariah M B 2016 *J. Alloy Compd.* **689** 199
[21] Bai J, Wang X S, Zu Q R, Zhao X and Zuo L 2016 *Acta Phys. Sin.* **65** 096103 (in Chinese)
[22] Chabungbam S and Sahariah M B 2015 *J. Alloy Compd.* **647** 70
[23] Chabungbam S, Gowtham S and Sahariah M B 2014 *Phys. Rev. B* **89** 085114
[24] Ozdemir Kart S and Cagın T 2010 *J. Alloy Compd.* **508** 177
[25] Li L J, Lei C H, Shu Y C and Li J Y 2011 *Acta Mater.* **59** 2648
[26] Wu P P, Ma X Q, Zhang J X and Chen L Q 2008 *J. Appl. Phys.* **104** 073906
[27] Wang J J, Ma X Q, Huang H B, He W Q, Liu Z H and Chen L Q 2013 *J. Appl. Phys.* **114** 013504
[28] Gu Y, Rabe K, Bousquet E, Gopalan V and Chen L Q 2012 *Phys. Rev. B* **85** 064117
[29] Kresse G and Hafner J 1993 *Phys. Rev. B* **47** 558
[30] Kresse G and Furthmüller J 1996 *Phys. Rev. B* **54** 11169
[31] Blöchl P E 1994 *Phys. Rev. B* **50** 17953
[32] John P, Perdew K B and Matthias Ernzerhof 1996 *Phys. Rev. Lett.* **77** 3865
[33] Methfessel M and Paxton A 1989 *Phys. Rev. B* **40** 3616
[34] Hobbs D, Kresse G and Hafner J 2000 *Phys. Rev. B* **62** 11556
[35] Marsman M and Hafner J 2002 *Phys. Rev. B* **66** 224409
[36] Togo A, Oba F and Tanaka I 2008 *Phys. Rev. B* **78** 134106
[37] Togo A and Tanaka I 2015 *Scr. Mater.* **108** 1
[38] Pérez-Landazábal J I, Recarte V, Sánchez-Alarcos V, Rodríguez-Velamazán J A, Jiménez-Ruiz M, Link P, Cesari E and Chumlyakov Y I 2009 *Phys. Rev. B* **80** 144301
[39] Shang S, Wang Y and Liu Z K 2007 *Appl. Phys. Lett.* **90** 101909
[40] Li C M, Luo H B, Hu Q M, Yang R, Johansson B and Vitos L 2012 *Phys. Rev. B* **86** 214205
[41] Voigt W 1928 *Lehrbuch der Kristallphysik* (Leipzig: Taubner Press)
[42] Reuss A and Angew Z 1929 *Math. Mech.* **9** 49
[43] Hill R 1952 *Proc. Phys. Soc. A* **65** 349
[44] Pugh S F 1954 *The London, Edinburgh, and Dublin Philosophical Magazine and Journal of Science* **45** 823
[45] Schroers J and Johnson W L 2004 *Phys. Rev. Lett.* **93** 255506
[46] Moruzzi V L, Janak J F and Schwarz K 1988 *Phys. Rev. B* **37** 790
[47] Herper E H and Entel P 1999 *Phys. Rev. B* **60** 3839
[48] James P, Eriksson O, Hjortstam O, Johansson B R and Nordström L 2000 *Appl. Phys. Lett.* **76** 915
[49] Enkovaara J, Ayuela A, Nordström L and Nieminen R 2002 *Phys. Rev. B* **65** 134422
[50] Wang H, Zhang Y N, Yang T, Zhang Z D, Sun L Z and Wu R Q 2010 *Appl. Phys. Lett.* **97** 262505
[51] Zayak A, Entel P, Enkovaara J, Ayuela A and Nieminen R 2003 *Phys. Rev. B* **68** 132402